Catalysis Science & Technology

ROYAL SOCIETY OF CHEMISTRY

PAPER

View Article Online
View Journal | View Issue

Cite this: *Catal. Sci. Technol.*, 2025, 15, 5452

One-pot synthesis of confined structure Ru_3Sn_7 alloys on alumina for exceptionally rapid and selective hydrogenolysis of furfuryl alcohol to 1,5-pentanediol†

Rodiansono, *[ab] Atina Sabila Azzahra,[a] Edi Mikrianto,[ab] Kiky Corneliasari Sembiring,[c] Ahmad Afandi,[d] Gagus Ketut Sunnardianto[e] and Indri Badria Adilina *[c]

A facile one-pot synthesis of confined structure Ruthenium–tin alloy catalysts on alumina ((op)Ru–(*x*)Sn@Al_2O_3) has been developed for highly efficient and selective synthesis of 1,5-pentanediol (1,5-PeD) from furfuryl alcohol (FFalc). A series of (op)Ru–(*x*)Sn@Al_2O_3 (*x* = Sn co-loading; 0.37–2.65 wt%) catalysts were synthesised *via* a one-pot coprecipitation-hydrothermal method of a solution containing ruthenium chloride and tin chloride and a hydrargillite-type of aluminium hydroxide ($Al(OH)_3$) at 150 °C for 24 h, followed by reduction with H_2 at 400 °C for 2 h. The (op)Ru–(1.30)Sn@Al_2O_3 catalyst obviously allowed the highest yield of 1,5-PeD (97%) with a productivity of 3.67 mmol 1,5-PeD per $g_{cat.}$per min from FFalc in water at 140 °C and 10 bar H_2, after 3 h. The presence of Ru_3Sn_7 or Ru–SnO_x catalysed the partial hydrogenation of the furan ring of FFalc to form 4,5-dihydrofuranmethanol (4,5-DHFM), and the acidic species of SnO_x or Sn^{n+} or acidic Al_2O_3 were used for activating C2–O for ring opening processes, while Ru^0 was used for the subsequent hydrogenation process, leading to high yield of the final 1,5-PeD product. This is the highest reported yield of 1,5-PeD from one-pot hydrogenolysis of FFalc under mild conditions. Catalytic performance of the recycled (op)Ru–(1.30)Sn@AL_2O_3 catalyst was restored after reactivation with H_2 at 400 °C for 1 h.

Received 6th May 2025,
Accepted 23rd July 2025

DOI: 10.1039/d5cy00542f

rsc.li/catalysis

1. Introduction

Alpha–omega (α,ω)-C5-diols (*e.g.*, 1,2-, 1,4- or 1,5-pentanediol (PeD)) have gained significant attention as versatile precursors for the production of various materials, including polyesters, polyurethanes, plasticizers, cosmetics, printing inks, and fungicides.[1,2] Among these (α,ω)-C5-diols, 1,5-PeD is particularly important and can be synthesised from C5-furans (*e.g.*, furfuraldehyde (FFald), furfuryl alcohol (FFalc), and tetrahydrofurfuryl alcohol (THFalc). However, achieving a high selectivity and high yield synthesis of 1,5-PeD from either FFald or FFalc is challenging due to the reactivity of the furan ring and the complex interactions on the catalyst surface.[3–5] Tomishige *et al.* highlighted that increasing the selectivity of 1,5-PeD or 1,2-PeD from FFalc is associated with metal active sites and the basicity or acidity of catalysts used.[6] Nevertheless, metal–acid catalysts with strong acidity led to the hydrogenative rearrangement of the furan ring to C5-cyclic compounds such as cyclopentanone (CPO) or cyclopentanol (CPL).[7] Consequently, designing and controlling catalyst behaviour to achieve high selectivity for 1,2-PeD or 1,5-PeD remains a significant challenge.

Catalysts based on supported precious metals such as Pt, Ir, Rh, Pd, or Ru, either in monometallic or bimetallic form, have been extensively investigated for the synthesis of 1,2-PeD and 1,5-PeD.[8–12] For instance, a Pt/CeO_2-nanocube catalyst with exposed (100) ceria-terminal facets produced a significantly higher yield of 1,2-PeD (77%) compared to Pt/CeO-nanorods and Pt/CeO-octahedron.[8] However, controlling the crystal plane of CeO_2 and the chemical state of Pt poses challenges for further fabrication and industrial application.

[a] *Catalysis for Sustainable Energy & Environment (CATSuRe), Inorganic Materials & Catalysis (IMCat) Laboratory, Lambung Mangkurat University, Indonesia. E-mail: rodiansono@ulm.ac.id*
[b] *Department of Chemistry, Lambung Mangkurat University, Jl. A. Yani Km 36, Banjarbaru, 70714, Indonesia. Tel: +62 511 477 3112*
[c] *Research Centre for Chemistry, BRIN, KST BJ Habibie, Serpong, Tangerang Selatan, Indonesia. E-mail: indr030@brin.go.id*
[d] *Research Centre for Advanced Materials, BRIN, KST BJ Habibie, Serpong, Tangerang Selatan, Indonesia*
[e] *Research Centre for Quantum Physics, BRIN, KST BJ Habibie, Serpong, Tangerang Selatan, Indonesia*

† Electronic supplementary information (ESI) available: Catalyst preparation & characterisation and catalytic reactions. See DOI: https://doi.org/10.1039/d5cy00542f

Additionally, a spinel-type $Pt/CoAl_2O_4$ catalyst, obtained through the coprecipitation method, was employed for the direct conversion of FFald. This catalyst yielded a mixture of 1,2-PeD (16%) and 1,5-PeD (35%) at 140 °C and 10 bar H_2 for 24 h.[13] Various Ir-, Rh-, Pd-, and Ru-based catalysts have also been developed by Tomishige and co-workers for the hydrogenolysis of FFald and its derivatives (*e.g.*, FFalc and THFalc) with a preference for higher selectivity of 1,5-PeD over 1,2-PeD.[11,14,15] They hypothesised that 1,5-PeD or 1,2-PeD was produced through the ring-cleavage of the saturated C–O bond in THFalc depending on the acidity or basicity of the catalyst systems.[16,17] Dumesic and co-worker proposed multi-step reaction pathways for 1,5-PeD synthesis from FFald, which involve total hydrogenation of FFald to THFalc by using Ni- or Ru-based catalysts, dehydration of THFalc to dihydropyran (DHP) on γ-Al_2O_3, hydration–tautomerisation–ring opening of DHP to 5-hydroxy valeraldehyde (5-HY-Val), and finally the hydrogenation of 5-HY-Val to 1,5-PeD on a Ru/C catalyst.[18] Since there are two competitive reaction pathways: the saturation of the C=C bond to form THFalc and the cleavage of the C–O bond leading to 1,2-PeD and 1,5-PeD, the exploration of heterogeneous catalysts that allow the one-step reaction of FFald or FFalc towards high yield of 1,5-PeD is still greatly challenging.

Several non-precious heterogeneous metal-based catalysts, including layered-double hydroxides or hydrotalcite structures have been intensively developed for the synthesis of 1,5-PeD from FFald or FFalc.[19–21] They proposed that controlling the basicity and increasing the density of low-coordination oxygen anions on the support led to higher basicity which facilitated the activation of the furan ring. For example, layered La-doped Cu–Co–Al hydrotalcites (LDHs),[19] the hydrotalcite-derived Ni–Co–Al,[20] and the Ni–$CoAlO_x$ (ref. 21) system with metallic Ni and $CoAlO_x$ demonstrated a synergistic action between Cu^0, CoO_x, and the basicity of metal oxides towards partial hydrogenation of the C=C furan ring, followed by the cleavage of the C2–O bond to selectively produce 1,5-PeD. The Cu–$Mg_3AlO_{4.5}$ catalyst can function as a bifunctional catalyst for the hydrogenolysis of FFalc, achieving an 80% yield of the 1,2-PeD and 1,5-PeD mixture.[22] Bimetallic oxides of perovskites or spinel structure catalysts such as CoO_x–PtO_x[23] and Co–CoO_x systems derived from MOFs,[24] and La-doped CuCoAl[25] systems, along with interfacial metal oxides and metals have preferentially interacted with the –CH_2OH group of FFalc. This interaction induced the C2–O oblique adsorption during the cleavage of the C2–O bond, leading to yield 1,5-PeD (40–60%) that was higher than 1,2-PeD. Specifically, the presence of the Cu–La interface in La-doped CuCoAl can simultaneously activate the furan ring and the –OH group in FFalc with an intermediate six-membered ring transition state, leading to high selectivity of 1,5-PeD with a yield up to 60% at 160 °C and 40 bar H_2 for 2 h.[25] Furthermore, Dai *et al.* claimed that the combination of balanced Cu^0–Cu^+ and Brønsted acid sites in the Cu/MFI catalyst afforded a 69% yield of 1,5-PeD at 160 °C and 25 bar H_2.[26] Wang *et al.* introduced a K promoter to form *x*K–Cu/MgO (*x* = 0–2 wt%), raising the yield of 1,5-PeD from 21% to 36% at 150 °C and 30 bar H_2 for 4 h.[27] Despite the development of several heterogeneous catalysts, the catalytic reactions inevitably produced moderate yield of 1,5-PeD (60%) with the yields of 1,2-PeD and THFalc still remaining noticeable.

Recently, we reported on bimetallic ruthenium–tin nanoparticles supported on gamma-alumina catalysts synthesised by a coprecipitation-hydrothermal method (Ru–(*y*)SnO_x/γ-Al_2O_3, where *y* represents the Sn co-loading; 0.65–2.15 wt%) for the aqueous phase hydrogenolysis of FFalc to 1,5-PeD. The Ru–(1.30)SnO_x/γ-Al_2O_3 catalyst, with a precise Sn co-loading, revealed the presence of Ru^0, Ru_3Sn_7 and SnO_x species that yielded exclusively 1,5-PeD (up to 94%) at 180 °C and 30 bar H_2 in H_2O after 7 h.[28] Attenuated total reflectance-infrared (ATR-IR) spectra of the reaction mixture under controlled reaction conditions exhibited a sharp absorption peak at 1637 cm^{-1}, which is assigned to trisubstituted C=C in the 4,5-dihydrofuranmethanol (4,5-DHFM) intermediate. This intermediate was consistently observed during the kinetic studies of reactions as shown in Scheme 1.[29] Furthermore, it was noted that THFalc was completely diminished alongside the evaluation of reaction parameters, suggesting a new reaction pathway for the formation of 1,5-PeD from FFald or FFalc that differs from the previously established pathways.[11,30]

Herein, we describe our extended investigation into the development of confined structure bimetallic Ru_3Sn_7 alloy catalysts supported on alumina for an exceptionally selective synthesis of 1,5-PeD from FFalc under mild conditions (140–160 °C, 10–20 bar H_2, and 3–6 h). The confined structure Ru_3Sn_7 catalysts on the alumina structure were synthesised using a one-pot coprecipitation-hydrothermal method (op), followed by reduction with H_2 at 400 °C for 2 h and produced the (op)Ru–(*x*)Sn@Al_2O_3 (*x* = Sn co-loading; 0.37–2.65 wt%) as shown in the schematic diagram (Fig. 1). Detailed experimental procedures of catalyst preparation, characterisation, and catalytic reactions are available in the ESI.† The reference Ru–(*x*)Sn/Al_2O_3 catalysts were synthesised using a coprecipitation-hydrothermal method (cop) producing (cop)Ru–(*x*)Sn/Al_2O_3-500 or (cop)Ru–(*x*)Sn/γ-Al_2O_3[28] and a wet-impregnation method (imp) producing (imp)Ru–(*x*)

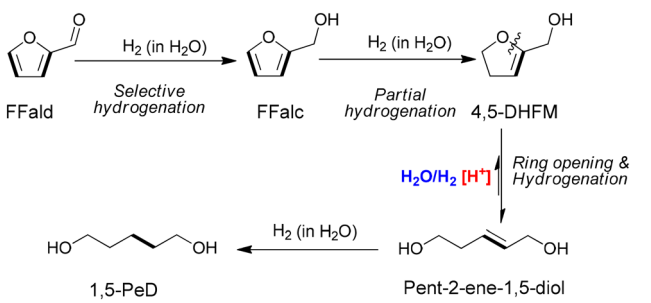

Scheme 1 Proposed reaction pathways of furfural into 1,5-PeD over bimetallic Ru–Sn alloy catalysts.[28]

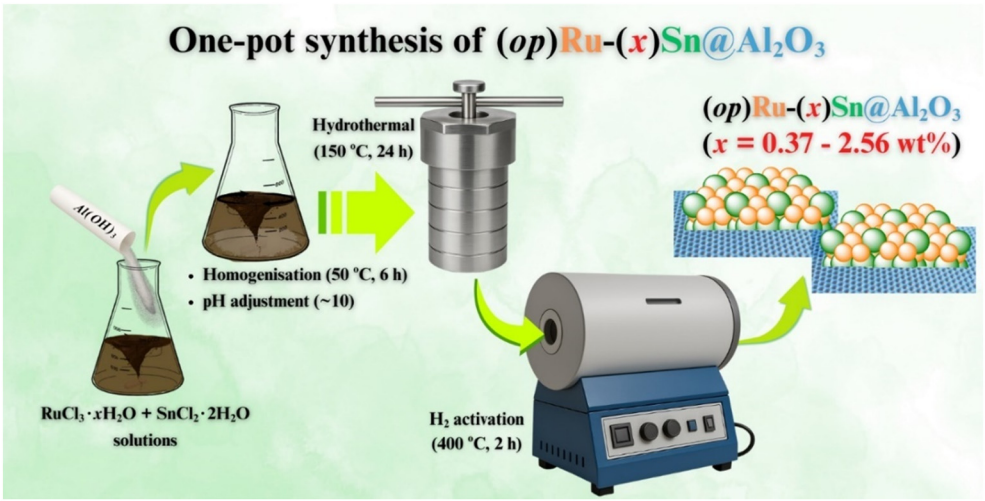

Fig. 1 Schematic diagram for the one-pot synthesis of confined structure Ru_3Sn_7 on alumina (Ru–(*x*)Sn@Al_2O_3; *x* = Sn co-loading (wt%)).

Sn/Al_2O_3-500. The (cop)Ru–(1.30)Sn@γ-Al_2O_3-500 catalyst achieved a yield of 81% for 1,5-PeD, whilst the (imp)Ru–(1.30)Sn@Al_2O_3-500 catalyst produced only 13%. Surprisingly, the (op)Ru–(1.30)Sn@Al_2O_3 catalyst gave the highest yield of 1,5-PeD at 97%. Although the catalytic performance of the recycled (op)Ru–(1.30)Sn@AL_2O_3 catalyst can be restored after the reactivation with H_2 at 400 °C for 1 h, the recyclability of the catalyst remains low. Therefore, systematic investigations to improve the recyclability of the catalyst after repeated reactions are essential for future investigation.

2. Results and discussion

2.1. Catalyst characterisation

A series of (op)Ru–(*x*)Sn@Al_2O_3 catalysts with different Sn co-loadings (*x* = 0.37–2.65 wt%) were synthesised by using a one-pot coprecipitation-hydrothermal method (op), followed by reduction with H_2 at 400 °C for 2 h, and the XRD patterns are shown in Fig. 2.

The sole structure of γ-Al_2O_3 or Al_2O_3 with a high intensity diffraction peak at 2θ = 67° is clearly observed in all samples (JCPDS #10-0425). This indicates that the $Al(OH)_3$ hydrargillite structure was perfectly transformed into γ-Al_2O_3 or Al_2O_3 during the catalyst preparation (see Fig. S1 in the ESI†). A series of sharp diffraction peaks at 2θ = 39.8, 43.5, 57.4, 72.1, and 85.7°, which can be attributed to Ru_3Sn_7(411), Ru_3Sn_7(420), Ru_3Sn_7(530), Ru_3Sn_7(721), and Ru_3Sn_7(653), respectively, were obtained (JCPDS #26-0504). The diffraction peaks of Ru_3Sn_7 alloy phases were intensified with an increase in Sn co-loading (Fig. 2(c and d)). The crystallite sizes of Ru_3Sn_7(411) at 2θ = 39.8° were determined to be 30.5 nm and 33.1 nm for (op)Ru–(1.30)Sn@Al_2O_3 and (op)Ru–(2.65)Sn@Al_2O_3 samples, respectively. The XRD patterns of the original $Al(OH)_3$ hydrargillite structure, along with its transformation into amorphous Al_2O_3 (γ-Al_2O_3) after calcination at 500 °C under N_2 for 2 h, are observed in Fig. S1(A), in the ESI.† The XRD patterns of monometallic (op) Ru@Al_2O_3 and (op)Sn@Al_2O_3 are shown in Fig. S1(B) in the ESI.† Additionally, the (cop)Ru–(1.30)Sn@Al_2O_3 sample exhibited a diffraction peak at 2θ = 43.6° suggesting the formation of the Ru_3Sn_7(420) alloy phase (Fig. S2(a) in the ESI†), whilst the (imp)Ru–(1.30)Sn@Al_2O_3 sample revealed Ru^0 species only (Fig. S2(b) in the ESI†). To gain insight into the existence of metallic Ru, Ru–Sn, and SnO_x species, X-ray photoelectron spectroscopy (XPS) analysis was performed on representative fresh and spent (op)Ru–(1.30)Sn@Al_2O_3 catalysts. The XPS spectra and the binding energies (BEs) of Ru $3d_{5/2}$ and Sn $3d_{5/2}$ in the fresh and spent (op)Ru–(1.30) Sn@Al_2O_3 are summarised in Fig. 3 and Table 1.

The signal of the Ru $3d_{3/2}$ orbital overlaps with that of the C 1s orbital; therefore, the Ru $3d_{5/2}$ peak was used to determine the chemical states of Ru species in all the

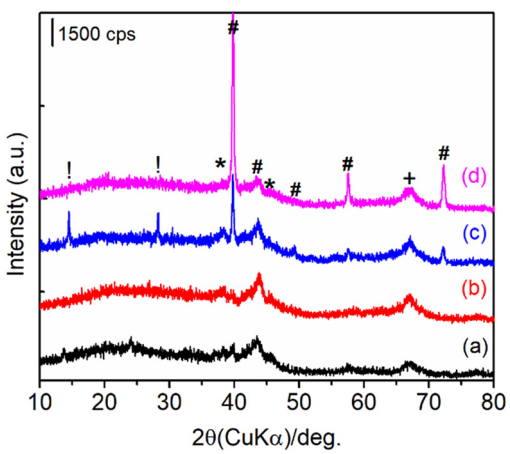

Fig. 2 XRD patterns of (op)Ru–(*x*)Sn@Al_2O_3 catalysts synthesised using a one-pot coprecipitation-hydrothermal methods with different Sn co-loadings (*x*) of (a) 0.37 wt%, (b) 0.65 wt%, (c) 1.30 wt%, and (d) 2.65 wt% after reduction with H_2 at 400 °C for 2 h. (!) bayerite/gibbsite; (*) Ru^0; (#) Ru_3Sn_7 alloy (JCPDS #26-0504); and (+) γ-Al_2O_3 (JCPDS #10-0425).

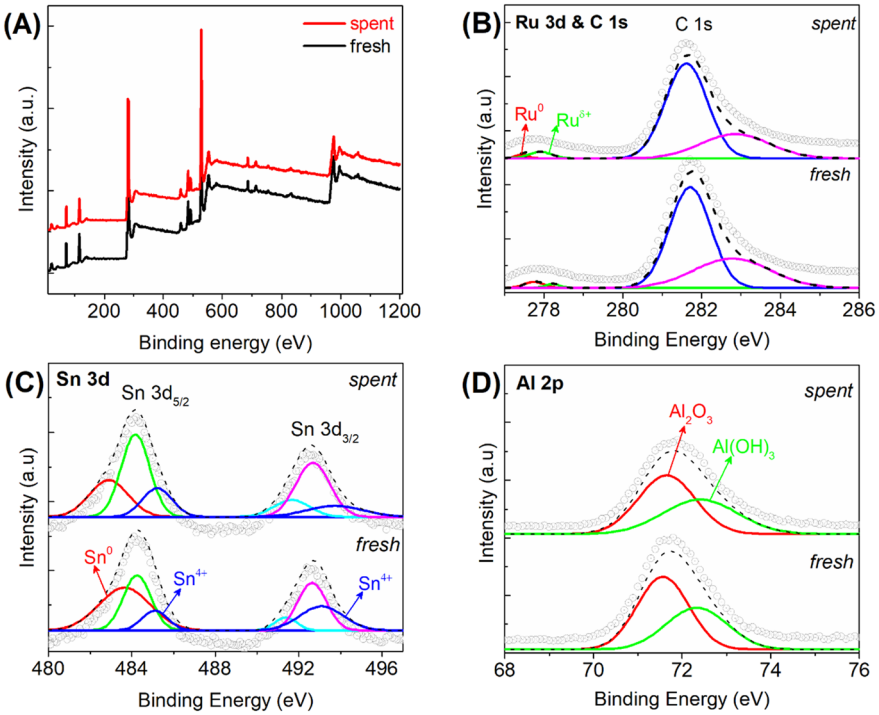

Fig. 3 XPS spectra of fresh and spent (op)Ru–(1.30)Sn@Al_2O_3 samples: (A) wide range spectra, (B) Ru $3d_{5/2}$, (C) Sn $3d_{5/2}$, and (D) Al 2p after reduction with H_2 at 400 °C for 2 h.

catalyst. The BEs of Ru $3d_{5/2}$ in both fresh and spent (op)Ru–(1.30)Sn@Al_2O_3 catalysts were observed at 277.82 eV and 277.75 eV, respectively, corresponding to the Ru^0 species. A peak between 278.61 and 278.68 eV was also observed, which can be attributed to the oxidative $Ru^{\delta+}$ species.[31] For the BE of Sn 3d, two centred peaks were identified: Sn $3d_{5/2}$ and Sn $3d_{3/2}$ at 484.66 eV and 493.01 eV, respectively, corresponding to oxidized Sn species ($Sn^{\delta+}$).[32] Additionally, there are weak shoulder peaks at 482.02 eV, 486.81 eV, and 494.18–494.37 eV detected in both fresh and spent (op)Ru–(1.30)Sn@Al_2O_3 samples, corresponding to reduced tin species (Sn^0) and Sn^{4+}, respectively. The BE of Ru $3d_{5/2}$ in the bimetallic Ru–Sn alloy was noticeably negatively shifted relative to that of monometallic Ru nanoparticles (BE Ru $3d_{5/2}$ = 279.75 eV).[33] The negatively shifted Ru $3d_{5/2}$ and Ru $3d_{3/2}$ peaks in spent (op)Ru–(1.30)Sn@Al_2O_3 indicate the charge transfer from Sn to Ru, resulting in the Ru atoms becoming negatively charged in the Ru–Sn alloy. Consequently, the affinity of Ru atoms in the Ru–Sn alloy towards C=C was greatly suppressed, leading to the inhibition of THFalc formation as clearly evidenced by the reaction profiles. Moreover, the BEs of Al 2p in Al_2O_3 (ranging from 71.57 to 71.65 eV) and $Al(OH)_3$ (72.33 to 72.44 eV) for both fresh and spent (op)Ru–(1.30)Sn@Al_2O_3 samples are clearly observed, with a slight decrease in the intensity of those species. This suggest that the Al_2O_3 or $Al(OH)_3$ species may leach into the reaction mixture.[28]

Table 1 Ru and Sn species information of fresh and spent (op)Ru–(1.30)Sn@Al_2O_3 detected by XPS

	Binding energy (eV)				
Sample	Ru^0 $3d_{5/2}$	$Ru^{\delta+}$ $3d_{5/2}$	Sn $3d_{5/2}$	Sn $3d_{3/2}$	Al 2p
Fresh	277.73	278.21	483.65 (Sn^0)	491.37	71.57
	282.77 (C 1s)		484.25	492.64	72.33
			485.11 (Sn^{4+})	493.10 (Sn^{4+})	
Spent	277.75	278.61	482.89	491.66	71.65
	282.60 (C 1s)		484.17	492.68	72.41
			485.22 (Sn^{4+})	493.73 (Sn^{4+})	

The physico-chemical properties of the representative catalysts, including bulk compositions, Brunauer–Emmet–Teller (BET) specific surface area (S_{BET}), H_2 uptake (derived from H_2-TPR data), and total acidity (derived from NH_3-TPD spectra), are summarised in Table 2. The SEM–EDS images and spectra of typical fresh and spent (op)Ru–(1.30)Sn@Al_2O_3 samples are presented in Fig. S3 and S4, in the ESI.† The N_2-adsorption–desorption and porosity profiles of three types of alumina supported Ru–(*x*)Sn alloy catalysts are shown in Fig. S5, in the ESI.† The Ru particle size estimated from the H_2 uptake using the proposed equation of Suib *et al.*[34] for the (op)Ru–(1.30)Sn@Al_2O_3 sample was 7.4 nm (entry 4). These are comparable with the average Ru nanoparticles obtained from HRTEM measurements (2.30 nm and 2.37 nm for fresh and spent, respectively) (see Fig. S6(a), in the ESI†) and the Scherrer equation at $2\theta = 39.8°$ (30.5 nm).

The NH_3-TPD profiles of the three types of synthesised Ru–(*x*)Sn@Al_2O_3 catalysts are shown in Fig. 4. The NH_3-TPD spectra were formally divided into three temperature regions for desorption, corresponding to three types of acid sites:[35] (1) weak acid sites, ranging from 100 to 200 °C, (2) moderate acid sites, ranging from 200 to 550 °C, and (3) strong acid sites, which are above 550 °C (Fig. S7, in the ESI†). The

Table 2 Physico-chemical properties of the synthesised (op)Ru–Sn(x)@Al_2O_3 catalysts

Entry	Catalyst[a]	Sn[b] (wt%)	Ru/Sn[b] (molar ratio)	S_{BET}[c] ($m^2\ g^{-1}$)	H_2[d] (mmol g^{-1})	Acidity[e] (mmol $NH_3\ g^{-1}$)	D[f] (%)	d_{va}[g] (nm)
1	(op)Ru@Al_2O_3	—	0	207	6.58	498	25.0	3.8
2	(imp)Ru–(1.23)Sn@Al_2O_3-500	1.23	3.6	192	3.59	537	14.4	6.3
3	(cop)Ru–(1.30)Sn@γ-Al_2O_3	1.30	3.2	158	5.48	798	22.0	4.1
4	(op)Ru–(1.30)Sn@Al_2O_3	1.30	3.4	142	3.03	750	12.1	7.4 (30.5)[h]
5	Rec. (op)Ru–(1.30)Sn@Al_2O_3	1.29	3.4	82	n.d.	n.d.	n.d.	n.d.

[a] The values in the parentheses are the amounts of Sn co-loading (wt%), determined by ICP-AES analysis. [b] Sn co-loading and Ru/Sn molar ratio were calculated from ICP-AES analysis data. [c] S_{BET} was derived from N_2 adsorption–desorption (BET method) at −196 °C. [d] H_2 uptake was derived from H_2-TPR spectra. [e] Acidity was derived from NH_3-TPD spectra. [f] Metal dispersion (%). [g] The Ru particle sizes (nm) were also estimated from the H_2 uptake data using the proposed equation of Suib *et al.* with an assumption that the surface area was occupied by an exposed (001) Ru surface.[34] [h] Values in the parentheses are the average crystallites sizes of the Ru_3Sn_7 alloy (2θ = 39.8°) calculated by the Scherrer equation. n.d. = not determined.

different synthetic procedures used for Ru–Sn may influence surface acidity, as reflected by the total acidity (measured in μmol NH_3 per gram) of each catalyst. The total acidity values for unmodified Ru@Al_2O_3, (imp)Ru–(1.23)Sn@Al_2O_3-500, (cop)Ru–(1.30)Sn@γ-Al_2O_3, and (op)Ru–(1.30)Sn@Al_2O_3 are 498 μmol NH_3 per gram, 537 μmol NH_3 per gram, 798 μmol NH_3 per gram, and 750 μmol NH_3 per gram, respectively (Fig. 4(A) and Table 2). Notably, the concentration of strong acidity in the (cop)Ru–(1.30)Sn@γ-Al_2O_3 and (op)Ru–(1.30)Sn@Al_2O_3 samples is significantly higher than that in the (imp)Ru–(1.23)Sn@Al_2O_3-500 and (op)Ru@Al_2O_3 samples (Fig. S7 and Table S1, in the ESI†). Since NH_3-TPD does not allow the differentiation of Lewis and Brønsted acid sites, pyridine-ATR-IR analysis was conducted on the three synthesised catalysts of (imp)Ru–(1.23)Sn@Al_2O_3-500, (cop)Ru–(1.30)Sn@γ-Al_2O_3, and (op)Ru–(1.30)Sn@Al_2O_3 (Fig. 4(B)). According to the literature on pyridine adsorption peaks in Sn-containing catalysts,[36,37] the bands are assigned as follows: the pyridinium ion (PyH^+), which forms from the reaction of pyridine with Brønsted acid sites (B), shows a band around 1647 cm^{-1} (ν_{8a}); coordinatively bound pyridines on Lewis acid sites (L) show bands around 1445 (ν_{19b}) and 1575 cm^{-1}; and physisorbed or hydrogen-bonded pyridine (H) exhibits bands at near 1437 and 1599 cm^{-1}. The band around 1490 cm^{-1} represents common vibrations from both PyH^+ (B) and coordinatively bound pyridine (L).[38] The Py-ATR-IR spectrum of (imp)Ru–(1.23)Sn@Al_2O_3-500 confirmed the sole presence of Lewis acid sites, indicated by bands at 1435, 1480, and 1580 cm^{-1}.[39] In contrast, the (cop)Ru–(1.30)Sn@γ-Al_2O_3 sample displayed the designed bands at 1647 cm^{-1}, signifying the presence of Brønsted acid sites. These Brønsted acid sites were likely generated by the presence of oxidic tin such as Sn(OH) or SnO_x during the catalyst preparation or during the catalytic reaction in the aqueous phase.[28,29,40,41]

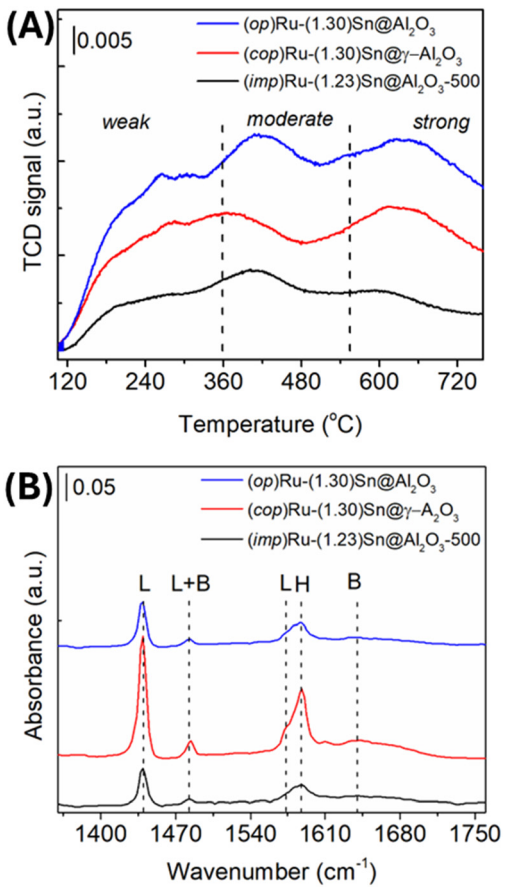

Fig. 4 (A) NH_3-TPD and (B) pyridine-ATR-IR profiles of Ru–(1.30)Sn@Al_2O_3 catalysts synthesised with different approaches after reduction with H_2 at 400 °C for 2 h.

2.2. Catalytic reactions

Effect of the synthesis procedure. Three (op)Ru–(1.30)Sn@Al_2O_3, (cop)Ru–(1.30)Sn@Al_2O_3, and (imp)Ru–(1.30)Sn@Al_2O_3 catalysts were prepared using different procedures. The catalysts were assessed for the conversion of FFalc to 1,5-PeD at 140 °C and 10 bar H_2 in water (H_2O) for 3 h and the results are shown in Fig. 5.

The (imp)Ru–(1.30)Sn@Al_2O_3-500 catalyst produced a yield of 75% for 2-pentanone (2-PeO) and 11% for 4,5-DHFM with low yield of 1,5-PeD (13%). The (cop)Ru–(1.30)Sn@Al_2O_3-500 catalyst achieved an 81% yield of 1,5-PeD, which is comparable to the Ru–(1.30)Sn/γ-Al_2O_3(E)

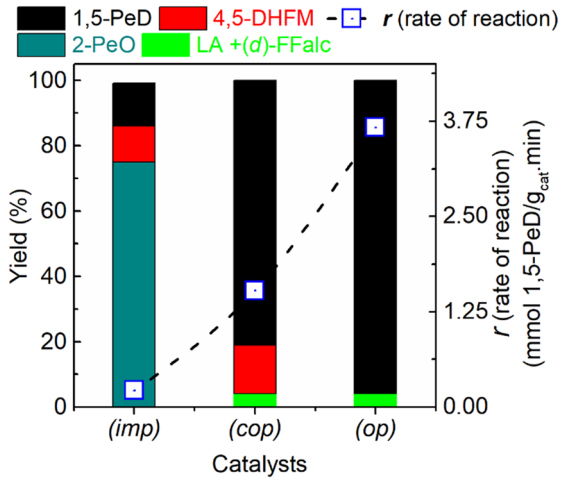

Fig. 5 Results of product distribution obtained from the FFalc reaction over three types of Ru–(1.30)Sn catalysts; namely (op)Ru–(1.30)Sn@Al_2O_3, (cop)Ru–(1.30)Sn@Al_2O_3, and (imp)Ru–(1.30)Sn@Al_2O_3 catalysts. Reaction conditions: catalyst, 50 mg; substrate (FFalc), 2.0 mmol; solvent (H_2O), 3 ml; initial H_2 pressure, 10 bar; 3 h.

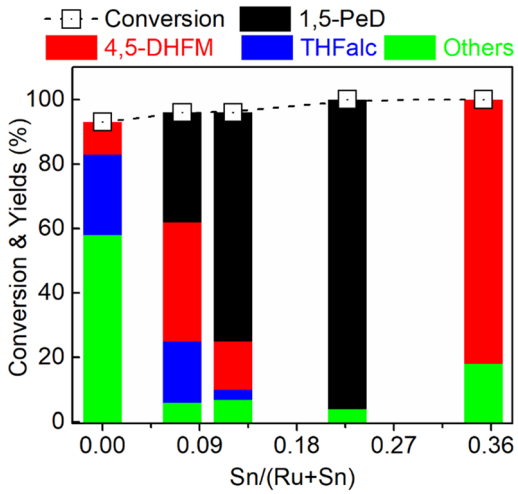

Fig. 6 Results of FFalc conversion and yields over (op)Ru–(*x*)Sn/Al_2O_3 catalysts with different Sn co-loadings. For the reaction conditions, refer to Fig. 5.

catalyst that produced 82% 1,5-PeD at 180 °C and H_2 30 bar after 3 h, as reported previously.[28] Other products included cyclopentanone (CPO), levulinic acid (LA), and a dimer of FFalc ((*d*)-FFalc). Surprisingly, the (op)Ru–(1.30)Sn@Al_2O_3 catalyst gave the highest yield of 1,5-PeD (97%), significantly higher than the yields obtained from FFald or FFalc over Ru–(1.30)Sn/ZrO_2 or Ru–(1.30)Sn/TiO_2 catalysts.[29] In addition, the superiority of the (op)Ru–(1.30)Sn@Al_2O_3 catalyst over other catalyst systems is clearly observed on the reaction rate of 1,5-PeD (mmol 1,5-PeD per g_{cat} per min). The reaction rate over the (op)Ru–(1.30)Sn@Al_2O_3 was measured at 3.67 mmol 1,5-PeD per g_{cat} per min, while the (cop)Ru–(1.30)Sn@Al_2O_3-500 and (imp)Ru–(1.30)Sn@Al_2O_3-500 catalysts showed lower rates of 1.53 mmol 1,5-PeD per g_{cat} per min and 0.22 mmol 1,5-PeD per g_{cat} per min, respectively. This calls for further evaluation of the effect of Sn co-loading, reaction parameters (temperature, initial H_2 pressure, and reaction profiles), and recyclability/reusability of the catalysts. Additionally, the possible reaction pathways of 1,5-PeD formation will be systematically investigated.

Effect of the Sn/Ru molar ratio. A series of (op)Ru–(*x*)Sn@Al_2O_3 catalysts with varying amounts of Sn co-loading were synthesised and evaluated for the catalytic conversion of FFalc to 1,5-PeD. The results are shown in Fig. 6.

Significant differences in product distributions were observed between (op)Ru@Al_2O_3 catalysts with and without Sn co-loading. The monometallic (op)Ru@Al_2O_3 catalyst (Ru = ~4 wt%) produced 25% THFalc, 10% 4,5-DHFM, and 58% by-products, which included CPO, levulinic acid LA, and a dimer of FFalc, based on GC–MS data. This was achieved at 93% conversion of FFalc at 140 °C and 10 bar H_2 for 3 h. When a small amount of Sn (0.37 wt%) was introduced to form (op)Ru–(0.37)Sn@Al_2O_3, the products were shifted to 34% 1,5-PeD, 37% 4,5-DHFM, 19% THFalc, and 6% by-products at 96% conversion of FFalc. Increasing the Sn co-loading to 0.64 wt% to form the (op)Ru–(0.64)Sn@Al_2O_3 catalyst further enhance the yield of 1,5-PeD to approximately two-folds (71%) at 96% conversion of FFalc, whereas the yields of 4,5-DHFM, THFalc, and by-products were 7%, 15%, 3%, and 7%, respectively. An impressive yield of 1,5-PeD (97%) at 100% conversion of FFalc was obtained over the (op)Ru–(1.30)Sn@Al_2O_3 (Sn = 1.30 wt%) catalyst whereas undesired THFalc had completely disappeared, indicating that the Ru–(1.30)Sn catalyst is inactive for complete hydrogenation of the furan ring. This can be attributed to the presence of Ru^0, Ru_3Sn_7 alloy, and SnO_x species, as clearly evidenced by the XRD patterns (Fig. 2) and XPS spectra of the (op)Ru–(1.30)Sn@Al_2O_3 catalyst (Fig. 3 and Table 1). Furthermore, the H_2 uptake and the metal dispersion data confirmed its high activity and selectivity (Table 1). We propose that the presence of metallic Ru^0, Ru_3Sn_7, Ru^0–SnO_x, oxidised Sn or SnO_x, molecular water, and acidic Al_2O_3 support work synergistically to catalyse the partial hydrogenation of C=C bonds and C2–O cleavage of the furan ring in FFalc during the aqueous phase reaction. The Ru^0–SnO_x species in the intermetallic Ru–Sn served as Brønsted acid or Lewis acid sites for the C2–O cleavage of FFalc or 4,5-DHFM, leading to the high yield of 1,5-PeD.[28,42] Additionally, the precise amount of Sn co-loading to form a bimetallic alloy or intermetallic Ni–Sn (ref. 30 and 43) or RANEY® Ni–Sn (ref. 44) catalysts considerably inhibited the hydrogenation of C=C bonds to THFalc and selectively catalysed FFald, FFalc, or 2-MeF to form 1,4-PeD in the H_2O/ethanol system.[45]

Effect of initial H_2 pressure. The influence of initial H_2 pressure on the conversion of FFalc and product distribution over the (op)Ru–(1.30)Sn@Al_2O_3 catalyst is shown in Fig. 7.

At an initial H_2 pressure of 5 bar, the main products were 45% 1,5-PeD and 37% 4,5-DHFM, alongside a small amount of 8% by-products (LA, CPO, and a dimer of FFalc) at 90% conversion of FFalc. As the initial H_2 pressure was increased

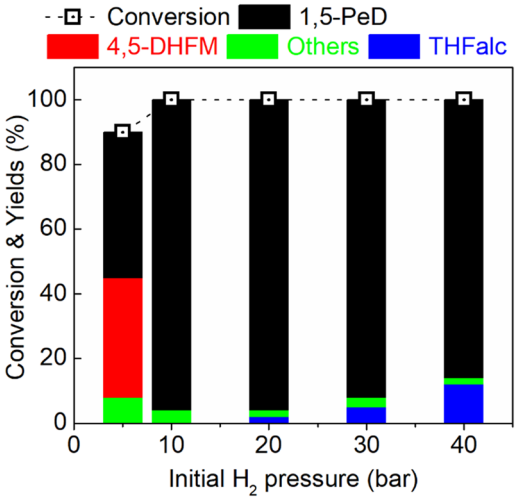

Fig. 7 Results of the FFalc conversion and yields over the (op)Ru–(1.30)Sn@Al_2O_3 catalyst as a function of initial H_2 pressure. For reaction conditions, refer to Fig. 5.

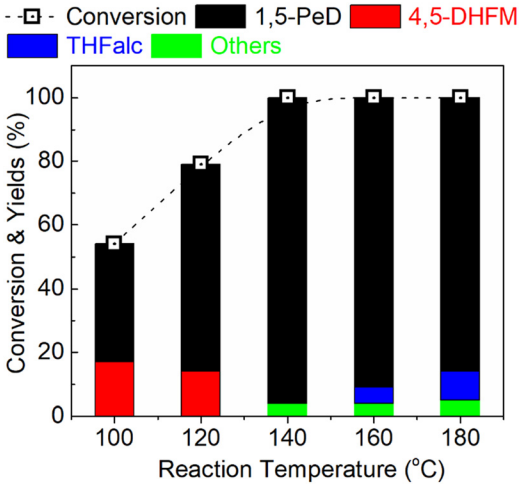

Fig. 8 Results of FFalc conversion and yields over the (op)Ru–(1.30)Sn@Al_2O_3 catalyst as a function of reaction temperatures. For reaction conditions, refer to Fig. 5.

to 10 bar, an outstanding yield of 1,5-PeD (97%) was obtained at 100% conversion of FFalc. At an initial H_2 pressure of 20 bar, the yield of 1,5-PeD remained the same at 10 bar, although the quantity of THFalc gradually increased at the higher H_2 pressure. This suggests that the elevated pressure promotes the complete hydrogenation of FFalc to produce THFalc. It has been reported that the C=C bond hydrogenation in FFald or FFalc to THFalc over Sn or In modified-Ni or Ru based catalysts tends to occur preferentially at high concentration of H_2.[44,46] In fact, the 1,5-PeD yields slightly decreased to 92% and 87% at the initial H_2 pressures of 30 and 40 bars, respectively, while the amounts of THFalc increased significantly to 5% and 12%. Thus, we concluded that the optimised initial H_2 pressure is between 10 and 20 bar.

Effect of reaction temperature. The influence of reaction temperature on product distribution in the one-pot conversion of FFalc over the (op)Ru–(1.30)Sn@Al_2O_3 catalyst is shown in Fig. 8.

At reaction temperatures of 100 °C and 120 °C, the conversions of FFalc were 54% and 79%, respectively, producing 1,5-PeD (27–65%) and 4,5-DHFM (14–17%) without any formation of THFalc. When the reaction temperature was increased to 140 °C, an extremely high yield of 1,5-PeD (96%) was obtained with only 4% of undesired product. However, further increasing the reaction temperature to 160 °C and 180 °C, the yield of 1,5-PeD slightly decreased to 91% and 86%, respectively, followed by a small amount of THFalc (5–9%) as the result of over hydrogenation of the C=C bond of FFalc. In addition, undesired by-products, including LA, CPO, 2-MeF, and 2-MeTHF, were also observed at these temperatures. It is well known that the formation of 2-MeF following the furan ring hydrogenation to 2-MeTHF occurs efficiently during the catalytic conversion of FFalc over mono- and bimetallic catalysts at higher temperature or at a low pressure of H_2.[44,47]

Survey of various alumina-supported Ru-Sn catalysts. The results of FFalc reactions over various synthesised Ru–(*x*)Sn@Al_2O_3 catalysts are summarised in Table 3. The (cop)Ru–(1.30)Sn/γ-Al_2O_3(*E*) catalyst gave a 100% conversion, yielding 44% 1,5-PeD and 22% 4,5-DHFM without any formation of THFalc. The reaction rate for 1,5-PeD formation (*r*) was 1.25 mmol 1,5-PeD per g_{cat} per min (entry 1). The (cop)Ru–(1.30)Sn/γ-Al_2O_3(H) catalyst yielded 19% 1,5-PeD, 20% 4,5-DHFM, 9% CPL and 18% undesired products (entry 2), while the (cop)Ru–(1.30)/γ-Al_2O_3(M) catalyst produced 58% 1,5-PeD at an 82% conversion of FFalc (entry 3). Furthermore, the (op)Ru–(2.56)Sn@Al_2O_3 catalyst (Sn co-loading = 2.56 wt%) produced 4,5-DHFM (82%) and other products (18%) at 100% conversion of FFalc (entry 4) (see Fig. S8(a), ESI†). As 4,5-DHFM is commercially unavailable, the reaction mixture from entry 4 was utilised to confirm the formation of 1,5-PeD from 4,5-DHFM. The used (op)Ru–(2.56)Sn@Al_2O_3 catalyst was removed through filtration and replaced with a fresh (op)Ru–(1.30)Sn@Al_2O_3 catalyst for further reaction at 140 °C and 10 bar H_2 for 3 h. Surprisingly, this process yielded a 75% production of 1,5-PeD, while 13% 4,5-DHFM remained and 12% by-products (including LA and a dimer of FFalc) were also identified (entry 5) (Fig. S8(b), ESI†). The as-prepared (op)Ru–(1.30)Sn@Al_2O_3 afforded 35% 1,5-PeD, 60% 4,5-DHFM, and 4% by-products (LA) achieving a notably high rate of 1,5-PeD formation (1.10 mmol 1,5-PeD per g_{cat} per min) (entry 6). Additionally, catalysts (cop)Sn/Al_2O_3-500 and Al_2O_3-500 were found to be inactive for the FFalc reaction to 1,5-PeD (entries 7 and 8). To confirm the presence of 4,5-DHFM, the catalytic reaction of FFalc in D_2O using (op)Ru–(1.30)Sn@Al_2O_3 was also performed. The GC chart and ^{1}H-NMR are shown in Fig. S9 and S10, in the ESI.† Results of the FFalc reaction over various supported Ru–(1.30)Sn catalysts, aside from alumina-based support, are summarised in Table S3, in the ESI.†

Table 3 Results of one-pot catalytic conversion of FFalc using bimetallic Ru supported on modified Al_2O_3 catalysts

Entry	Catalysts[a]	Conv.[b] (%)	Yield[b] (%)					r^d (rate of reaction)
			1,5-PeD	4,5-DHFM	CPO (CPL)	THFalc	Others[c]	
1	(cop)Ru–(1.30)Sn/γ-Al_2O_3(E)	66	44	22	0	0	0	1.25
2	(cop)Ru–(1.30)Sn/γ-Al_2O_3(H)	68	19	20	9	0	19	0.85
3	(cop)Ru–(1.30)Sn/γ-Al_2O_3(M)	82	58	6	7	5	5	1.28
4	(op)Ru–(2.56)Sn@Al_2O_3	100	0	82	0	0	18	n.d.
5[e]	(op)Ru–(1.30)Sn@Al_2O_3	100	75	13	0	0	12	2.22
6	As prepared (op)Ru–(1.30)Sn@Al_2O_3	99	35	60	0	0	4	1.10
7	(cop)Sn/Al_2O_3-500	35	—	—	—	—	35	n.d.
8	Al_2O_3-500	15	—	—	—	—	15	n.d.

Reaction conditions: catalyst, 50 mg; substrate (FFalc), 2.0 mmol; solvent (H_2O), 3 ml; initial H_2 pressure, 10 bar; 140 °C, 3 h.[a] The values in the parentheses are the loading amounts of Sn (wt%). [b] Conversion and yield were determined by GC (FID) using an internal standard technique. [c] By-products include LA and a dimer of FFalc ((*d*)-FFalc) (based on the GC-MS data). [d] *r* (rate of reaction; mmol 1.5-PeD per g_{cat} per min). [e] The reactant was the reaction mixture obtained from a reaction run using the (op)Ru–(2.56)Sn@Al_2O_3 catalyst (entry 4). The carbon balance was more than 96% for all the catalysts.

Effect of second metals. The effects of various second metal (*e.g.*, In, Cu, Co, Mo) and active metal (*e.g.*, Pd and Ni) catalysts on the conversion of FFalc and the yield of 1,5-D were evaluated, and the results are summarised in Table S2, in the ESI.† Notably, the (op)Ru–(1.30)In@Al_2O_3 catalyst showed promising results, achieving 57% yield of 1,5-PeD at 71% conversion of FFalc (entry 1), and this catalyst is currently under investigation. In contrast, other bimetallic Ru- and Pd-based catalysts demonstrated poor selectivity for 1,5-PeD (entries 2–6). Sn-modified Ni or RANEY® Ni-based catalysts primarily produced 1,4-PeD under similar reaction conditions (160 °C, 30 bar H_2, 3–12 h) (entries 7–10), as reported in previous study.[30,43,44] The effects of various supported Ru–(1.30)Sn catalysts on FFalc conversion and 1,5-PeD yield were also investigated (see Table S3, in the ESI†). Typically, acidic (*e.g.*, γ-Al_2O_3, AC, TiO_2) supported Ru–(1.30)Sn catalysts gave 1,5-PeD (entries 1–3); meanwhile, basic (*e.g.*, Nb_2O_5, ZnO, MgO) supported Ru–(1.30)Sn catalysts afforded higher yield of 1,2-PeD compared to 1,5-PeD (entries 4–6), which aligns with the findings from previous studies by Upare *et al.*[48] and Mizugaki *et al.*[49] Only the (cop)Ru–(1.30)Sn/ZrO_2 catalyst afforded moderate yield of 1,5-PeD (64%) while leaving 32% of 4,5-DHFM unreacted under the same conditions (entry 7). Further investigation of this catalyst is ongoing and will be reported in a subsequent publication. We carried out the reaction of FFalc in the presence of 10 mmol% pyridine as a poison using the (cop)Ru–(1.30)Sn@Al_2O_3-500 catalyst at 140 °C and 10 bar H_2 for 3 h. The conversion of FFalc was only 11% for producing a dimer of FFalc without the formation of 4,5-DHFM and 1,5-PeD. This result indicates that the presence of pyridine inhibited both the hydrogenation of the C=C bond and ring opening of the C–O bond (entry 11, Table S2, and Fig. S13, in the ESI†).

Time profiles & ATR-IR study. The reaction profiles for the one-pot conversion of FFalc over the (op)Ru–(1.30)Sn@Al_2O_3 catalyst were studied at 140 °C with an initial H_2 pressure of 10 bar over a time span of 0 to 6 h, as shown in Fig. 9.

At an early reaction time of 0.5 h, about 48% of FFalc was converted to 21% 1,5-PeD, 26% 4,5-DHFM and 4% LA + (*d*)-FFalc. Both the conversion of FFalc and yield of 1,5-PeD increased simultaneously as the reaction time was prolonged to 1 h. The maximum yield of 4,5-DHFM and LA + (*d*)-FFalc reached 23% and 7%, respectively, at 0.5–0.75 h, after which they plateaued after 2 h. The reaction was completed (100% conversion of FFalc) after 1.5 h, with the yield of 1,5-PeD gradually increasing to maximum (97%) after 4 h, leaving a remaining amount of 3% LA. These results indicate that the formation of 1,5-PeD occurs at a faster rate than that of 4,5-DHFM. Once 4,5-DHFM is formed on the catalyst surface, it rapidly undergoes hydrogenolysis *via* C2–O scission to form 1,5-PeD on Ru_3Sn_7 and Ru–SnO_x species. The partial hydrogenation of the furan ring was also affected by the concentration of adsorbed H_2 on the surface, as indicated by results in Fig. 7 regarding the effect of the initial H_2 pressure.

As shown in Fig. 9, 4,5-DHFM was clearly observed at the early stage of the reaction but completely disappeared after 6 h. Moreover, the amounts of by-products slightly

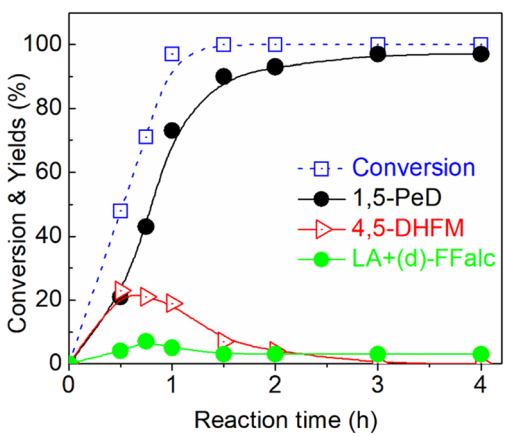

Fig. 9 Time profiles for the one-pot conversion of FFalc and yields over the (op)Ru–(1.30)Sn@Al_2O_3 catalyst.

increased during the initial phase of the reaction (0.5–0.75 h), remaining unchanged (~3%) even after 6 h. It is possible that the formation of an oligomer from FFalc and LA occurred due to the surface acidity of Ru–SnO_x or Al_2O_3 as the reaction time was prolonged.[50] Therefore, it can be presumably concluded that the formation of 1,5-PeD from FFalc follows a typical pattern of consecutive reaction pathways. To support this suggestion, specific reaction conditions (140 °C and 2.5 bar H_2 for 0.5–3.0 h in a trace amount of H_2O (2–3 drops)) were used and monitored using ATR-IR spectroscopy, and the results are shown in Fig. 10.

The ATR-IR spectra of the reaction mixture showed that an asymmetric band of C=C in 4,5-DHFM was observed at 1633 cm^{-1} and the band intensified over time. Firstly, adsorbed FFalc on the Ru_3Sn_7 or Ru–SnO_x surface of (op)Ru–(1.30)Sn@Al_2O_3 was partially hydrogenated to form the 4,5-DHFM intermediate. The formed 4,5-DHFM was further activated by Brønsted acid sites of Ru–SnO_x or Al_2O_3 support at the C2–O bond, while the terminal –OH group attached to SnO_x or Al_2O_3. These promoted the cleavage of the C2–O bond, leading to the formation of penta-2-ene-1,5-diol, which is rapidly hydrogenated to form 1,5-PeD as the final product (Scheme 2).[13,28,51] While our mechanistic interpretations are supported by *ex situ* characterization and literature, future research could incorporate *in situ* DRIFTS and XAS/EXAFS to provide deeper insights into the adsorption configurations of intermediates like 4,5-DHFM and the real-time evolution of C–O bond cleavage on Ru–Sn sites.

Substrate scope. To evaluate the reactivity of the (op)Ru–(1.30)Sn@Al_2O_3 catalyst, catalytic reactions were performed using several substrates; FFald, hydroxymethylfurfural (HMF), 2,5-dimethylfuran (2,5-DMF), 2-MeF, and 2,3-dihydromethylfuran (2,3-DHMF), and the results are summarised in Table 4. For FFald, the catalyst produced 65% 1,5-PeD, 20% FFalc, 9% 4,5-DHFM, and 5% other products, which is comparable with (cop)Ru–(1.30)Sn/γ-Al_2O_3 (entry 1).[28] In a separate reaction, 97% of 2-MeF was converted to 57% *n*-pentanol, 34% 2-MeTHF, and 6% 1,4-PeD (entry 2). These results align with the previous conversion of 2-MeF to 1,4-PeD using the Ni_3Sn@AlOH catalyst.[45] The reaction of 2,5-DMF produced 34% 2,5-hexanediol, 9% 2,5-hexanedione, 21% 2,5-dimethyltetrahydrofuran (2,5-DMTHF), and 2-hexanol (10%), resulting in a conversion of 74% 2-DMF (entry 3).[52] The homolog 2,3-dihydro-5-methylfuran (2,3-DHMF) was reacted over the (op)Ru–(1.30)Sn@Al_2O_3 catalyst at 140 °C and an initial H_2 pressure of 10 bar for 3 h. 65% 2,3-DHMF was converted to produce 42% *n*-pentanol (PeOH), 20% 2-methyltetrahydrofuran (2-MeTHF), and 3% 1,4-PeD (entry 4). Additionally, the (op)Ru–(1.30)Sn@Al_2O_3 catalyst showed no activity for the reaction of THFalc (entry 5). Based on these reaction results, along with the observed kinetic profiles and substrate scope, it can be inferred that the plausible reaction pathways for the selective transformation of FFalc to high yield of 1,5-PeD over bimetallic Ru–(*x*)Sn catalysts are consistent with previously established pathways.[29,53,54]

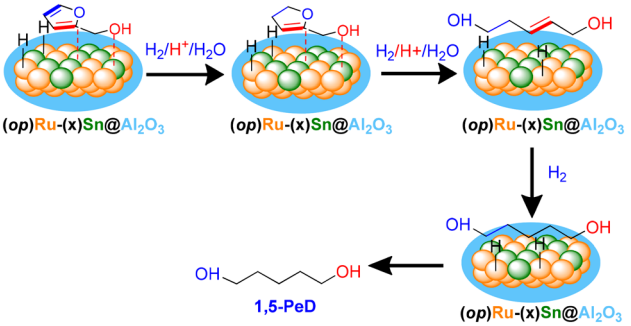

Scheme 2 Plausible reaction pathways for the selective synthesis of 1,5-PeD from FFalc in the presence of the bimetallic (op)Ru–(1.30) Sn@Al_2O_3 catalyst in H_2O.

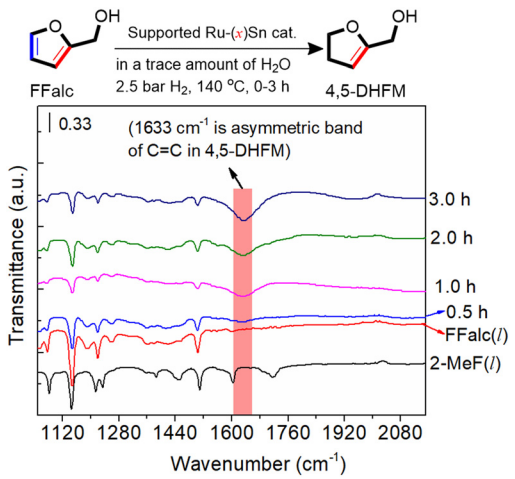

Fig. 10 ATR-IR spectra of the reaction mixtures (slurry) of FFalc (5 drops) in the presence of a trace amount of H_2O (3 drops) over the (op)Ru–(1.30)Sn@Al_2O_3 catalyst (50 mg) at 140 °C and 2.5 bar H_2 for 0.5–3.0 h.

Recyclability and reusability tests. Recyclability and reusability tests were performed for the (op)Ru–(1.30) Sn@Al_2O_3 catalyst and the results are shown in Fig. S11, in the ESI.† The conversion of FFalc remained at 100%, while the yield of 1,5-PeD slightly decreased to around 80% after the 3rd reaction run. The amount of 4,5-DHFM slightly increased after repeated reaction runs, while the yield of by-products remain unchanged. These may be attributed to the presence of partial oxidative species of either Ru^0 to RuO_2 or Sn^0 to SnO_x on the surface of the Ru_3Sn_7 alloy, as well as the presence of Al_2O_3 and $Al(OH)_3$ phases according to the XPS profiles (Fig. 2(C–F)). This is consistent with the SEM-EDS data (Fig. S2(b) and S3(b)†) and the TEM images (Fig. S6, in the ESI†) during the reusability test. The presence of a significant number of oxidative species of RuO_2 or SnO_x contributed to a high yield of 4,5-DHFM, which was depicted by the reaction results of the as-prepared (op)Ru–(1.30)Sn@Al_2O_3 (Table 2, entry 8) and high Sn co-loading

Table 4 Results of substrate scope reactions using the (op)Ru–(1.30)Sn@Al_2O_3 catalyst

Entry	Substrate	Conversion[a] (%)	Products[a] (% yield)			
1		100 ± 0.49	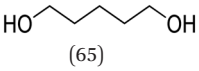 (65)	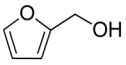 (20)	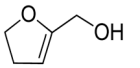 (9)	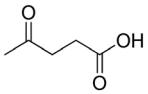 (6)
2		97 ± 0.62	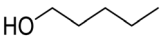 (57)	 (34)	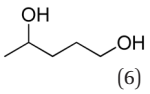 (6)	—
3	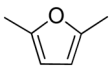	74 ± 0.43	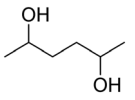 (34)	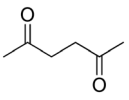 (9)	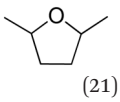 (21)	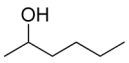 (10)
4		65 ± 0.51	 (42)	 (20)	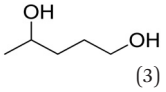 (3)	—
5	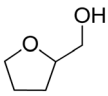	No reaction	—	—	—	—

Reaction conditions: catalyst, 50 mg; substrate, 2.0 mmol; solvent (H_2O), 3 ml; initial H_2 pressure, 10 bar; 140 °C, 3 h.[a] Conversion and yield were determined by GC (FID) using an internal standard technique. Values in the parentheses are the yield of the product. The carbon balance was more than 98% for all the reactions.

(op)Ru–(2.56)Sn@Al_2O_3 catalysts (Table 2, entry 6). In addition, the Al_2O_3 or $Al(OH)_3$ structure may partially leach out into the reaction mixture during the reaction under hydrothermal conditions, as noted by Huo *et al.*[55] and Schüth *et al.*[56] The XRD patterns of the recovered catalysts revealed that the sole structure of Al_2O_3 or γ-Al_2O_3 and Ru_3Sn_7 alloy phases after the third reaction remain unchanged, confirming its high stability (Fig. S12, in the ESI†). Surprisingly, after the reactivation of the recycled catalyst with H_2 at 400 °C for 1–2 h, followed by passivating with N_2 for 15 min, the high yield of 1,5-PeD was restored (94%), which is comparable to the fresh catalyst. Inductively coupled-plasma (ICP) analysis of the reaction mixture after the third reaction run confirmed that small amounts of Sn (1.3 mol%) and Al (0.78 mol%) were present in the filtrate while Ru was negligible.

3. Conclusion

In conclusion, we have developed a facile one-pot synthesis of the confined structure Ru_3Sn_7 alloy on alumina ((op)Ru–(*x*)Sn@Al_2O_3) catalysts which demonstrated exceptionally rapid and selective hydrogenolysis of FFalc towards 1,5-PeD under mild conditions (140 °C, 10–20 bar H_2, 3–6 h). For comparison, two types of (cop)Ru–(1.30)Sn/γ-Al_2O_3 and (imp)Ru–(1.30)Sn/Al_2O_3 catalysts were also synthesised using coprecipitation (cop) and wet impregnation (imp), respectively. The (imp)Ru–(1.30)Sn@Al_2O_3-500 produced only 13% yield of 1,5-PeD, whilst the (cop)Ru–(1.30)Sn@Al_2O_3-500 catalyst produced 81% 1,5-PeD; meanwhile, the (op)Ru–(1.30)Sn@AL_2O_3 catalyst afforded an outstanding yield of 97% 1,5-PeD, with a productivity of 3.67 mmol 1,5-PeD per g_{cat} per min. This result represents the highest yield and selectivity for 1,5-PeD compared to the state-of-the-art catalysts in the one-pot conversion of FFalc to diols under milder conditions. In the (op)Ru–(1.30)Sn@Al_2O_3 catalyst, the presence of Ru_3Sn_7 or Ru–SnO_x facilitates the partial hydrogenation of the furan ring in FFalc to form 4,5-DHFM. The acidic species of SnO_x or Sn^{n+} or acidic Al_2O_3 promote the activation of ring opening processes *via* C2–O cleavage, while Ru^0 is used for the following hydrogenation, leading to the high yield of the final product 1,5-PeD. This synthetic strategy can guide the design of more-efficient, selective, and stable catalysts for the catalytic direct conversion of furfural or furfuryl alcohol to 1,5-pentanediol.

Data availability

The data supporting this article have been included as part of the ESI.†

Author contributions

Rodiansono: conceptualisation, methodology, writing – original draft, writing – review & editing, and supervision. Atina Sabila Azzahra and Edi Mikrianto: formal analysis (XPS and XRD), investigation, and experiment. Indri Badria Adilina, Kiky Corneliasari Sembiring, Gagus Ketut Sunnardianto, and Ahmad Afandi: writing – review & editing,

supervision, and formal analysis (XPS, NH_3-TPD, H_2-TPR, and N_2-adsorption analyses).

Conflicts of interest

There are no conflicts to declare.

Acknowledgements

The authors acknowledge The Indonesian Endowment Funds for Education (LPDP) through BRIN-RIIM2 scheme (contract number of 79/IV/KS/11/2022), DRPTM-Kemendiktisaintek through Regular Fundamental scheme (contract number of 056/E5/PG.02.00.PL/2024), and LPPM-ULM through Internal Fundamental scheme (contract number of 1374.95/UN8.2/PG/2024) for financial support. We also acknowledge the facilities and scientific and technical support from the Advanced Chemical Characterization Laboratory, National Research, and Innovation Agency through E- Layanan Sains - BRIN.

Notes and references

1 M. Schlaf, *Dalton Trans.*, 2006, 4645–4653.
2 R. Gérardy, D. P. Debecker, J. Estager, P. Luis and J. C. M. Monbaliu, *Chem. Rev.*, 2020, **120**, 7219–7347.
3 Y. Zhu, W. Zhao, J. Zhang, Z. An, X. Ma, Z. Zhang, Y. Jiang, L. Zheng, X. Shu, H. Song, X. Xiang and J. He, *ACS Catal.*, 2020, **10**, 8032–8041.
4 M. J. Gilkey, A. V. Mironenko, L. Yang, D. G. Vlachos and B. Xu, *ChemSusChem*, 2016, **9**, 3113–3121.
5 J. He, K. Huang, K. J. Barnett, S. H. Krishna, D. M. Alonso, Z. J. Brentzel, S. P. Burt, T. Walker, W. F. Banholzer, C. T. Maravelias, I. Hermans, J. A. Dumesic and G. W. Huber, *Faraday Discuss.*, 2017, **202**, 247–267.
6 K. Tomishige, M. Honda, H. Sugimoto, L. Liu, M. Yabushita and Y. Nakagawa, *Carbon Neutrality*, 2024, **3**, 1–41.
7 X. Li and Q. Deng, *Trans. Tianjin Univ.*, 2023, **29**, 347–359.
8 T. Tong, X. Liu, Y. Guo, M. N. Banis, Y. Hu and Y. Wang, *J. Catal.*, 2018, **365**, 420–428.
9 Z. Wang, B. Pholjaroen, M. Li, W. Dong, N. Li, A. Wang, X. Wang, Y. Cong and T. Zhang, *J. Energy Chem.*, 2014, **23**, 427–434.
10 J. Guan, G. Peng, Q. Cao and X. Mu, *J. Phys. Chem. C*, 2014, **118**, 25555–25566.
11 S. Liu, Y. Amada, M. Tamura, Y. Nakagawa and K. Tomishige, *Green Chem.*, 2014, **16**, 617–626.
12 L. Bruna, M. Cardona-Farreny, V. Colliere, K. Philippot and M. R. Axet, *Nanomaterials*, 2022, **12**, 1–11.
13 W. Xu, H. Wang, X. Liu, J. Ren, Y. Wang and G. Lu, *Chem. Commun.*, 2011, **47**, 3924–3926.
14 Y. Nakagawa and K. Tomishige, *Catal. Today*, 2012, **195**, 136–143.
15 S. Koso, N. Ueda, Y. Shinmi, K. Okumura, T. Kizuka and K. Tomishige, *J. Catal.*, 2009, **267**, 89–92.
16 D. Sun, S. Sato, W. Ueda, A. Primo, H. Garcia and A. Corma, *Green Chem.*, 2016, **18**, 2579–2597.
17 X. Li, P. Jia and T. Wang, *ACS Catal.*, 2016, **6**, 7621–7640.
18 Z. J. Brentzel, K. J. Barnett, K. Huang, C. T. Maravelias, J. A. Dumesic and G. W. Huber, *ChemSusChem*, 2017, **10**, 1351–1355.
19 J. Tan, Y. Su, X. Hai, L. Huang, J. Cui, Y. Zhu, Y. Wang and Y. Zhao, *Mol. Catal.*, 2022, **526**, 112391.
20 J. Peng, D. Zhang, Y. Wu, H. Wang, X. Tian and M. Ding, *Fuel*, 2023, **332**, 126261.
21 Q. Shen, Y. Li, F. Wang, X. Zhang, Z. Zhang, Z. Zhang, Y. Yang, C. Bing, X. Fan, J. Zhang and X. He, *Mol. Catal.*, 2024, **556**, 113919.
22 H. Liu, Z. Huang, F. Zhao, F. Cui, X. Li, C. Xia and J. Chen, *Catal. Sci. Technol.*, 2016, **6**, 668–671.
23 D. Liu, J. Fu, J. Wang, X. Zhu, J. Xu, Y. Zhao and J. Huang, *Appl. Surf. Sci.*, 2024, **642**, 158571.
24 T. Xiang, D. Dai, X. Li, D. Liu, C. Feng, P. Dai, L. Li, X. Gu and Y. Liu, *Appl. Catal. B: Environ.*, 2024, **348**, 123841.
25 J. Tan, H. Huang, Y. Zhang, J. Cui, J. Zhang, L. Huang, Y. Wang and Y. Zhu, *Green Chem.*, 2024, **26**, 11608–11624.
26 D. Dai, C. Feng, M. Wang, Q. Du, D. Liu, Y. Pan and Y. Liu, *Catal. Sci. Technol.*, 2022, **12**, 5879–5890.
27 J. Wang, D. Liu, X. Yao, J. Fu, S. Jia and J. Huang, *Appl. Catal., A*, 2024, **676**, 119675.
28 R. Rodiansono, A. S. Azzahra, U. T. Santoso, E. Mikrianto, E. Suarso, K. C. Sembiring, I. B. Adilina, G. K. Sunnardianto and A. Afandi, *Catal. Sci. Technol.*, 2025, **15**, 808–821.
29 R. Rodiansono, A. S. Azzahra, E. Mikrianto, A. Ridhoni, I. Mustari, A. Nurfitriani, T. S. D. Bodoi, R. E. Sanjaya, E. Suarso and P. R. Ansyah, *Bull. Chem. React. Eng. Catal.*, 2025, **20**, 293–306.
30 R. Rodiansono, M. D. Astuti, T. Hara, N. Ichikuni and S. Shimazu, *Green Chem.*, 2019, **21**, 2307–2315.
31 Z. Yang, Y. Xiong, T. Li, Z. Yang and B. H. Chen, *Catal. Commun.*, 2024, **186**, 106822.
32 M. J. Hidajat, I. T. Ghampson, G.-N. Yun and D. W. Hwang, *Chem. Eng. J.*, 2023, **461**, 141912.
33 D. J. Morgan, *Surf. Interface Anal.*, 2015, **47**, 1072–1079.
34 X. Shen, L.-J. Garces, Y. Ding, K. Laubernds, R. P. Zerger, M. Aindow, E. J. Neth and S. L. Suib, *Appl. Catal., A*, 2008, **335**, 187–195.
35 J. Wang, P. A. Chernavskii, Y. Wang and A. Y. Khodakov, *Fuel*, 2013, **103**, 1111–1122.
36 E. Tututi-Ríos, H. González, D. A. Cabrera-Munguia, A. Gutiérrez-Alejandre and J. L. Rico, *Catal. Today*, 2022, **394–396**, 235–246.
37 A. Rezayan, K. Wang, R. Nie, T. Lu, J. Wang, Y. Zhang and C. C. Xu, *Chem. Eng. J.*, 2022, **429**, 132261.
38 M. Tamura, K. I. Shimizu and A. Satsuma, *Appl. Catal., A*, 2012, **433–434**, 135–145.
39 C. Martin, I. Martin, C. Delmoral and V. Rives, *J. Catal.*, 1994, **146**, 415–421.
40 L. Ma, H. Wang, C. Zhu, Q. Liu, J. Tan, C. Wang and Z. Liang, *ChemSusChem*, 2019, **12**, 2154–2160.
41 X. Liu, X. Liu, G. Xu, Y. Zhang, C. Wang, Q. Lu and L. Ma, *Green Chem.*, 2019, **21**, 5647–5656.
42 R. Ma, X.-P. Wu, T. Tong, Z.-J. Shao, Y. Wang, X. Liu, Q. Xia and X.-Q. Gong, *ACS Catal.*, 2017, **7**, 333–337.

43 R. Rodiansono, A. S. Azzahra, P. R. Ansyah, S. Husain and S. Shimazu, *RSC Adv.*, 2023, **13**, 21171–21181.
44 R. Rodiansono, M. D. Astuti, K. Mustikasari, S. Husain, P. R. Ansyah, T. Hara and S. Shimazu, *RSC Adv.*, 2022, **12**, 241–250.
45 R. Rodiansono, M. D. Astuti, S. Husain, A. Nugroho and S. Sutomo, *Bull. Chem. React. Eng. Catal.*, 2019, **14**, 529–541.
46 R. Rodiansono, M. D. Astuti, D. R. Mujiyanti, U. T. Santoso and S. Shimazu, *Mol. Catal.*, 2018, **445**, 52–60.
47 Y. Yang, L. Chen, Y. Chen, W. Liu, H. Feng, B. Wang, X. Zhang and M. Wei, *Green Chem.*, 2019, **21**, 5352–5362.
48 P. P. Upare, Y. Kim, K. R. Oh, S. J. Han, S. K. Kim, D. Y. Hong, M. Lee, P. Manjunathan, D. W. Hwang and Y. K. Hwang, *ACS Sustainable Chem. Eng.*, 2021, **9**, 17242–17253.
49 T. Mizugaki, T. Yamakawa, Y. Nagatsu, Z. Maeno, T. Mitsudome, K. Jitsukawa and K. Kaneda, *ACS Sustainable Chem. Eng.*, 2014, **2**, 2243–2247.
50 D. Götz, M. Lucas and P. Claus, *React. Chem. Eng.*, 2016, **1**, 161–164.
51 Q. Liu, B. Qiao, F. Liu, L. Zhang, Y. Su, A. Wang and T. Zhang, *Green Chem.*, 2020, **22**, 3532–3538.
52 Y. L. Louie, J. Tang, A. M. L. Hell and A. T. Bell, *Appl. Catal., B*, 2017, **202**, 557–568.
53 T. S. D. Bodoi, A. S. Azzahra, M. R. Ansyari, E. Mikrianto, R. Rodiansono, R. E. Sanjaya and P. R. Ansyah, *1st ICWDGs 2024, AIP Conference Proceedings*, 2024, pp. 325–338.
54 A. S. Azzahra, N. Annisa, R. Rodiansono, U. T. Santoso, R. E. Sanjaya and E. Suarsa, *1st ICWSDGs 2024, AIP Conference Proceedings*, 2024, pp. 127–138.
55 J. Huo, J.-P. Tessonnier and B. H. Shanks, *ACS Catal.*, 2021, **11**, 5248–5270.
56 A. P. Amrute, K. Jeske, Z. Łodziana, G. Prieto and F. Schüth, *Chem. Mater.*, 2020, **32**, 4369–4374.